JOURNAL OF MATERIALS SCIENCE 26 (1991) 5741–5752

Morphological characterization of microcellular carbon foams

J. H. AUBERT, A. P. SYLWESTER
Sandia National Laboratories, Albuquerque, NM 87185, USA

Microcellular carbon foams have been prepared by the high-temperature carbonization of polyacrylonitrile (PAN) foams in an inert atmosphere. The PAN precursor foams were first prepared by thermally induced phase separation of PAN solutions followed by gelation/extraction or freezing/freeze-drying processes. The resulting carbon foams have low densities and open-celled morphologies. We have developed two complementary techniques to characterize objectively carbon foam morphologies, BET surface area measurements and mercury porosimetry. These two measurement techniques, when used in conjunction with known stereological rules, allow us to calculate densities and average cell sizes or cell size distributions. As a bonus, values of the bulk modulus for low-density carbon foams also can be determined from mercury porosimetry. Unlike other techniques, our determinations do not require carefully prepared surfaces (such as for microscopy) or an assumed morphological model (required for most other techniques).

1. Introduction

Low-density, microcellular carbon foams have been developed for a variety of uses that include catalyst supports, adsorbents, porous electrodes and other battery components, high-temperature insulation, and as a material used in some high-energy physics experiments such as inertial confinement fusion. The microcellular foams of interest for such applications have cell sizes in the range 0.1–20 μm. This range is usually about one to three orders of magnitude smaller than foams made by conventional techniques such as the expansion of polymer/blowing agent mixtures. Our method to prepare these foams is by the high-temperature degradation of polyacrylonitrile (PAN) foams in an inert atmosphere [1, 2]. The PAN foams are initially prepared by the controlled thermally induced phase separation (TIPS) of PAN solutions followed by solvent removal. Two alternative techniques have been recently described to prepare low-density, microcellular carbon foams. Both involve carbonization of an organic foam which was prepared either by a replication process [3, 4] or from an organic aerogel [5]. To design and use these carbon foams effectively, it is necessary to characterize their morphology. In this paper, we describe two techniques which are well suited to characterize microcellular carbon foam morphologies. We will demonstrate these two characterization techniques with carbon foams prepared with the PAN TIPS process.

Thermally induced phase separation (TIPS) of polymer solutions is a versatile technique to prepare low-density microcellular polymer foams. The process consists of three steps [6]. In the first step, a polymer and solvent are heated above their critical temperature to achieve a homogeneous polymer solution. The second step consists of quenching the solution in a controlled fashion to initiate thermally induced phase separation. Under some circumstances, TIPS can result in the formation of bi-continuous phases, a polymer-rich phase and a solvent-rich phase. In the third step the bi-continuous phases are frozen in place which effectively terminates the phase separation. The solvent can then be sublimed, which removes the solvent and leaves the polymer behind as the continuous solid phase of the foam. Alternatively, with semi-crystalline polymers the solution may form a stable gel after TIPS. In this case, the third step can either be to freeze the gel and sublime the solvent or else to remove the solvent super-critically. A successful technique with gels is to extract the solvent with another solvent (such as acetone or methanol) which in turn is extracted with super-critical carbon dioxide. Fig. 1 schematically shows the TIPS process. TIPS allows a range of foam properties to be obtained. For example, foam densities can be varied from about 0.02–0.2 g cm^{-3}. As we will demonstrate below, cell sizes can be varied from submicrometre to about 20 μm.

After the PAN foams have been prepared from the TIPS process, they can be carbonized. Prior to carbonization, however, PAN foams are thermally pretreated in air [7]. This step results in the cyclization of PAN to the "ladder polymer" structure shown in Fig. 2. Optimal pretreatment conditions for the PAN foams were determined to be 220 °C for 16–24 h in air [2]. Pretreated PAN foams are then carbonized at high temperature in an argon atmosphere (either 1100 or 1200 °C for the foams described in this work). This results in formation of a rigid low-density, carbonized, microcellular foam which retains the same morphol-

0022–2461/91 $03.00 + .12

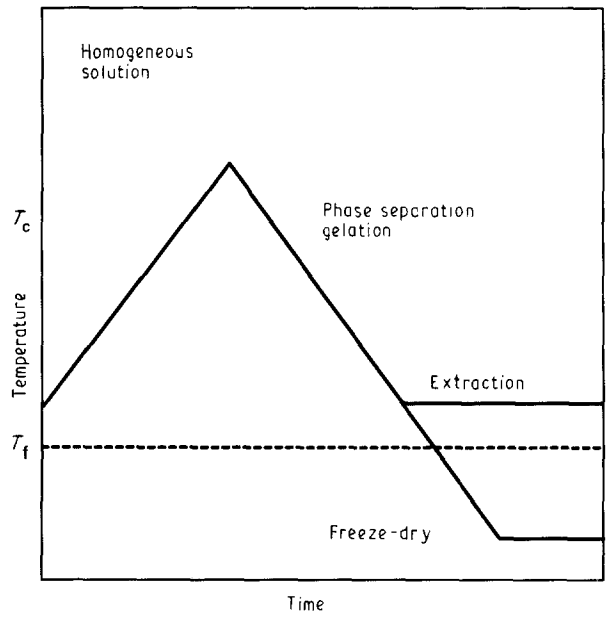

Figure 1 Schematic illustration of the TIPS process to prepare a microcellular polymer foam. T_c is the critical temperature for phase separation. T_f is the freezing point of the solvent, if applicable.

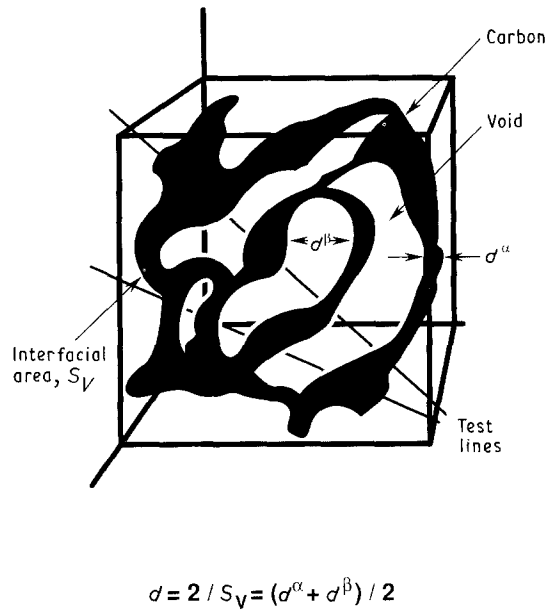

$$d = 2 / S_V = (d^{\alpha} + d^{\beta}) / 2$$

Figure 3 Schematic drawing of microcellular foam morphology with surface area per unit volume, S_V. Random test lines are shown intersecting the foam surfaces as could be done to calculate the "cell size" manually.

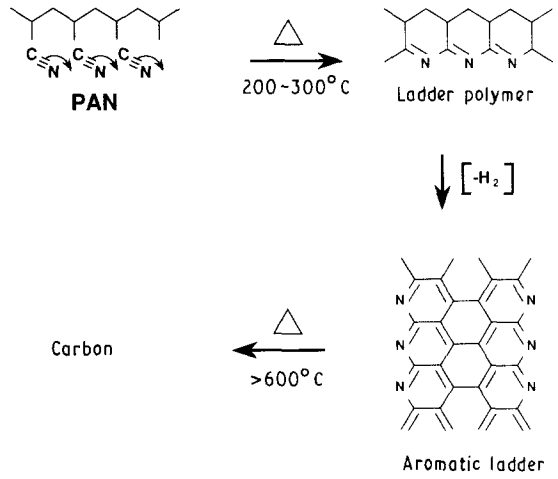

Figure 2 PAN carbonization chemistry.

ogy as the initial PAN foam precursor. The final properties of the carbon foams depend upon the actual thermal treatment [1, 2].

The TIPS process results in foam morphologies with no real "cellular" character, i.e. no spherical voids. Commonly, an open and strut-like or sheet-like morphology is observed. Fig. 3 schematically shows a typical carbon foam morphology prepared with the PAN process. To use these materials effectively in any of the applications it is necessary to characterize the cells that are present in the material. Many of the traditional methods of characterizing the cells require an a priori assumption as to the geometry of the cells. For example, mercury porosimetry usually relies upon the assumption that the pores are cylindrical. ASTM standard D-3576-77 describes a technique for determining the cell size of conventional foams, but it requires an assumption of spherical cells. Microscopy allows one to observe the foam morphology directly. However, the image may depend upon how the foam surface was prepared. In addition it is very difficult to quantify any image obtained. The limitations of these and other techniques to quantify the cell size of microcellular foams has been discussed previously [8].

We have found that one useful measure of the "cell size" is the average spacing between surfaces in the foam, d. The average spacing between surfaces can be thought of as a generalized "cell size". In theory, this could be calculated by passing a line through the foam and measuring the distances between intersections of the line and foam. If one did this for all solid angles and determined the average, then the result would be d. A well-known stereological relationship provides an exact relationship between d and the interfacial area per unit volume, S_V, of the material [8]. For low-density foams this relationship takes the form

$$d = 4/S_V \quad (1)$$

In a typical application of Equation 1, one would measure d from a photograph (scanning electron photomicrograph) and then calculate S_V [9]. Our approach has been to measure S_V directly, with either BET nitrogen adsorption (Brunauer, Emmett and Teller theory [10]) or mercury porosimetry, and then to calculate d. BET nitrogen adsoprtion gives a single surface area, and therefore a single value for the cell size is obtained. Mercury porosimetry can give the cell size distribution. These two techniques are well suited to characterize the morphology of microcellular carbon foams. Neither technique requires any a priori assumption as to the morphology of the foam. Know-

ing the cell size distribution allows carbon foams (prepared in different ways) to be objectively compared. This aids in the development of microcellular foams, allows the cell size distribution to be compared to models of foam formation, and allows the performance of the carbon foam in a given application to be related to the morphology of the foam.

2. Experimental procedure

BET surface areas were measured with a Quantachrome Monosorb model surface area analyser (Quantachrome, Syosset, NY). This instrument uses the single-point method. We have previously shown that the single-point method gives values of surface area within 6% of a multipoint determination [8] for similar open-celled polymer foams. The reproducibility of the measurements was shown to be well within this 6% error. The technique results in a single value for the surface area, which from Equation 1 results in a single average cell size. We define this as the surface area average cell size, $\langle d \rangle_S$. For foams with a monodisperse cell size, we have shown previously that this technique results in cell sizes that correlate extremely well with those observed by scanning electron microscopy. For foams that are not monodisperse, the average corresponds to

$$\langle d \rangle_S = [\Sigma d_i S_i]/\Sigma S_i \quad (2)$$

where S_i is the surface area of foam made up of cells of size d_i. In other words, this average weights each cell size by the surface area of those cells.

Mercury porosimetry was performed with a Quantachrome Autoscan-500 Porosimeter. The technique involves forcing mercury into a foam by the application of pressure. The fundamental measurements are the volume of mercury intruded as a function of the applied pressure.

Carbon foams were prepared by the thermal decomposition of PAN foams as described above. All of the foams investigated were carbonized at either 1100 or 1200 °C. This temperature was high enough to anneal any porosity occurring within the struts or sheets of the foam [2]. Hence, values of surface areas or volume of mercury intruded corresponded to the cells of interest and not defects within the solid phase of the foams. Density measurements were performed by volume and weight determinations on foams with machined surfaces.

3. Theory

Mercury porosimetry involves forcing mercury into the cells of a foam with pressure. An energy balance on the process (which is not dependent upon the morphology) equates the pressure–volume work to the surface work [10]

$$P\,dV_i = -\gamma_{lv}\cos\theta\,dS_i \quad (3)$$

where γ_{lv} is the liquid–vapour interfacial tension of mercury (480 dyn cm^{-1} [10]) and θ is the wetting angle (approximately 154.9° for carbon [10]). dV_i is the differential volume of foam filled at pressure P corresponding to that part of the foam with cell size d_i and corresponding to a differential surface area of dS_i. A typical intrusion curve is shown in Fig. 4. Because mercury does not wet the foam's surface, work must be performed to fill the cells. Large cells require less work to fill than do smaller cells, and hence larger cells fill at lower pressures. Rearranging Equation 3 shows that the surface area per unit volume as a function of pressure is directly obtained in the experiment

$$S_{V_i} = dS_i/dV_i = -P/\gamma_{lv}\cos\theta \quad (4)$$

The surface area per unit volume of cells that fill at pressure P is defined as S_{V_i}. Hence, the fundamental quantity obtained in a mercury porosimetry experiment is the surface area per unit volume. The total surface area of the foam is obtained by multiplying Equation 4 by V_i and summing over all measured points (or integrating for a continuous distribution of data points)

$$S = \Sigma(-P\,V_i/\gamma_{lv}\cos\theta) \quad (5)$$

The surface area average cell size is obtained by combining Equations 1 and 5

$$\langle d \rangle_S = \Sigma V_i/\Sigma(-P\,V_i/4\,\gamma_{lv}\cos\theta) \quad (6)$$

Combining Equations 1 and 4 gives the average distance between surfaces, d_i, of those cells in the foam that would be intruded with mercury at pressure, P

$$d_i = 4/S_{V_i} = -4\gamma_{lv}\cos\theta/P \quad (7)$$

Mercury porosimetry is also capable of determining the cell size distribution (volume of cells as a function of cell size, d_i). The cell size distribution requires no a priori morphological assumption.

A useful average cell size is the volume average, $\langle d \rangle_V$, which weights the large cells very heavily

$$\langle d \rangle_V = \Sigma(d_i V_i)/\Sigma V_i = \Sigma(-4\gamma_{lv}\cos\theta\,V_i/P)/\Sigma(V_i) \quad (8)$$

The volume average and the surface area average cell sizes will give different averages for all except monodisperse celled-sized foams. Because the volume, V_i, goes as d_i^3 and the surface area, S_i, goes as d_i^2, these averages involve the ratio of different moments of the cell size distribution. The volume average goes as the ratio of the fourth to the third moment, and the surface area average goes as the ratio of the third to the second moment,

$$\langle d \rangle_V \sim \Sigma n_i(d_i)^4/\Sigma n_i(d_i)^3 \quad (9a)$$

$$\langle d \rangle_S \sim \Sigma n_i(d_i)^3/\Sigma n_i(d_i)^2 \quad (9b)$$

where n_i is the number of cells with size d_i. The volume average is always larger than the surface area average. The ratio of the volume average to the surface area average, $\langle d \rangle_V/\langle d \rangle_S$, is a measure of the breadth of the cell-size distribution.

Another measure of the breadth of the cell-size distribution that we will report is the volume-based

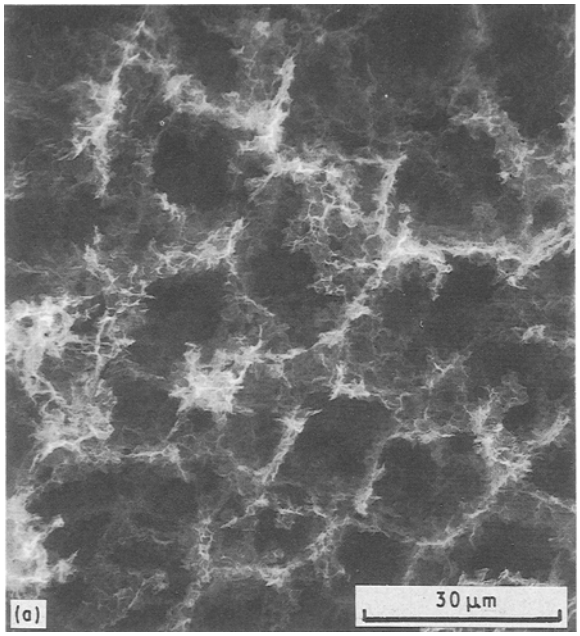

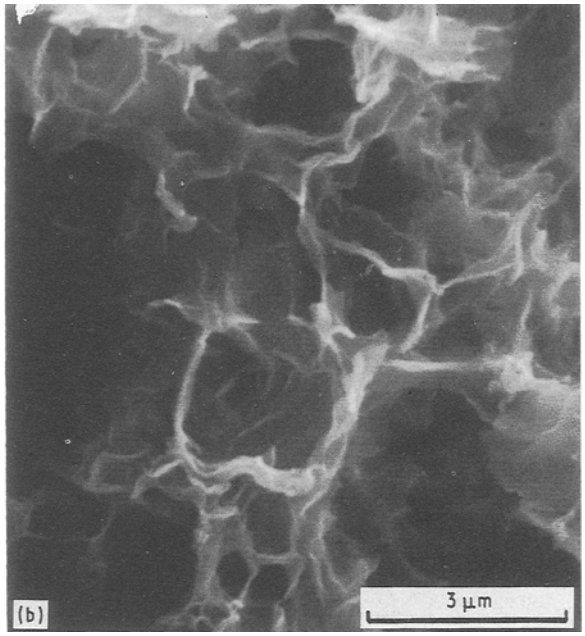

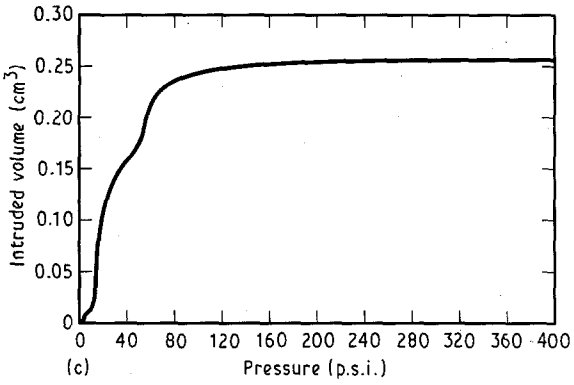

Figure 4 An example of a mercury intrusion curve for one microcellular carbon foam of density 0.045 g cm^{-3}. Both the scanning electron photomicrographs and the intrusion curve show the bimodal morphology. $\langle d\rangle_V = 11.69$ μm, $\langle d\rangle_S = 6.62$ μm, $\sigma_V/\langle d\rangle_V = 0.69$, $\rho_{Hg} = 45.3$ mg cm^{-3}. 10^3 p.s.i. = 6.89 N mm^{-2}.

standard deviation

$$\sigma_V = [\Sigma V_i(d_i - \langle d\rangle_V)^2/\Sigma V_i]^{0.5} \quad (10)$$

Any other standard deviation could also be defined in a similar way based upon a different average, such as the surface area average, $\langle d\rangle_S$. Table I summarizes the definitions that will be reported on carbon foams from either BET nitrogen adsorption or mercury porosimetry. Fig. 5 shows some model intrusion curves and the calculated cell size averages and standard deviations.

4. Discussion

Note that the expression in Equation 7 is identical to that obtained in two other ways. The traditional interpretation of mercury porosimetry data involves an analysis of Equation 3 using the assumption of cylindrical pores [10]. With that assumption, $dS_i/dV_i = 4/d_i$, where d_i is the cylindrical diameter. Substituting this expression in Equation 3 surprisingly gives the same result as in Equation 7. This equation is much more general, however, and is not limited to the cylindrical geometry assumption. In fact the usefulness of mercury porosimetry is almost certainly a result of this more general interpretation of the cell size because very few porous media have cylindrical pores; yet, mercury porosimetry has been very successful in giving meaningful values for cell sizes.

Another measure of cell size in a random porous medium is the hydraulic radius. This is particularly relevant for flow in porous media. The hydraulic radius is defined as the ratio of the wetted volume to the wetted surface area, $r_{hi} = dV_i/dS_i$. Using Equation 4 we have for the hydraulic radius

$$r_{hi} = dV_i/dS_i = -\gamma_{lv}\cos\theta/P \quad (11)$$

The cell diameter is four times the hydraulic radius [11] which results in the identical expression for the diameter as in Equation 7

$$d_i = 4r_{hi} = -4\gamma_{lv}\cos\theta/P \quad (12)$$

TABLE I Calculated statistical quantities from BET nitrogen adsorption and mercury porosimetry

BET nitrogen adsorption	$\langle d\rangle_{SBET} = 4/S_{VBET}$
Mercury porosimetry	$\langle d\rangle_{SHg} = \Sigma V_i/\Sigma(-PV_i/4\gamma_{lv}\cos\theta)$
	$\langle d\rangle_V = \Sigma(-4\gamma_{lv}\cos\theta V_i/P)/\Sigma(V_i)$
	$\langle d\rangle_V/\langle d\rangle_{SHg}$
	$\sigma_V = [\Sigma V_i(d_i - \langle d\rangle_V)^2/\Sigma V_i]^{0.5}$

To differentiate between equivalent quantities that can be determined from either BET nitrogen adsorption or mercury porosimetry, such as S_V and $\langle d\rangle_S$, we further subscript these terms to indicate which experimental value is used. We can then compare these quantities. S_{VBET}/S_{VHg}; $\langle d\rangle_{SBET}/\langle d\rangle_{SHg}$.

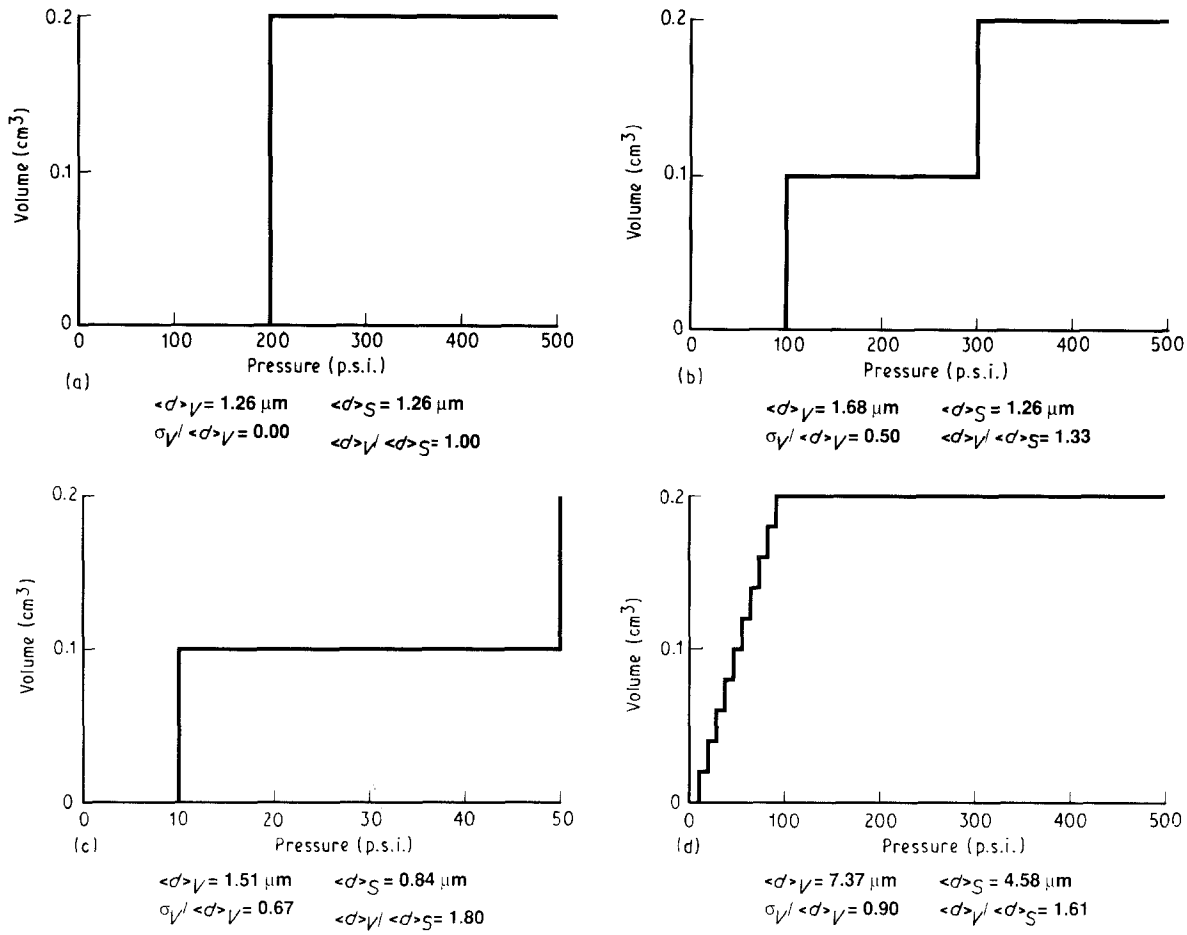

Figure 5 Model intrusion curves and the associated cell size averages and standard deviations; (a) monodisperse, (b) bimodal, (c) broader bimodal, and (d) broad distribution.

Hence, four times the hydraulic radius is exactly the average distance between surfaces, as defined above.

Although mercury porosimetry can be analysed without any a priori morphological assumptions, it is necessary to correct the experimental data for two common artefacts. The artefacts are due to surface defects (which appear as very large cells in the intrusion curve) and bulk compression of the foam sample which occurs during the pressurization. These two artefacts must be removed from the data prior to the cell size distribution analysis. Fig. 4 contains an experimental intrusion curve, the calculated surface area average and volume average cell sizes, and a scanning electron photomicrograph. Both the photomicrograph and the intrusion curve show that the cell size distribution is bimodal. The artefact due to surface defects appears as a jump in the intrusion curve occurring at the origin. Fig. 6 shows a schematic intrusion curve, which although slightly exaggerated, has the features typical of the carbon microcellular foams.

The surface filling artefact can be verified by looking at different sized samples of the same carbon foam. Fig. 7 shows three intrusion curves for a single carbon foam that was prepared with three different sample sizes. The large piece of foam, which has little external surface, displays only a small jump at the origin. The normal sized piece shows the typical sized jump at the origin. The final example was a foam cut up into many small pieces. This sample shows an extraordinary jump at the origin, which if not accounted for would dominate the cell size distribution. Clearly these examples show that the jump at the origin in the intrusion curve is due to the external surface of the foam and the defects within this surface. The volume associated with filling the cracks or large defect voids on the external sample surface must be eliminated from the calculations of the cell size distribution and also from the

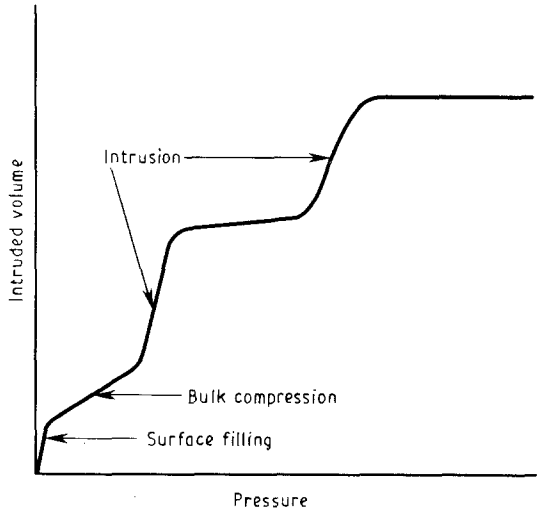

Figure 6 Schematic intrusion curve showing the artefacts due to external surface filling and bulk compression.

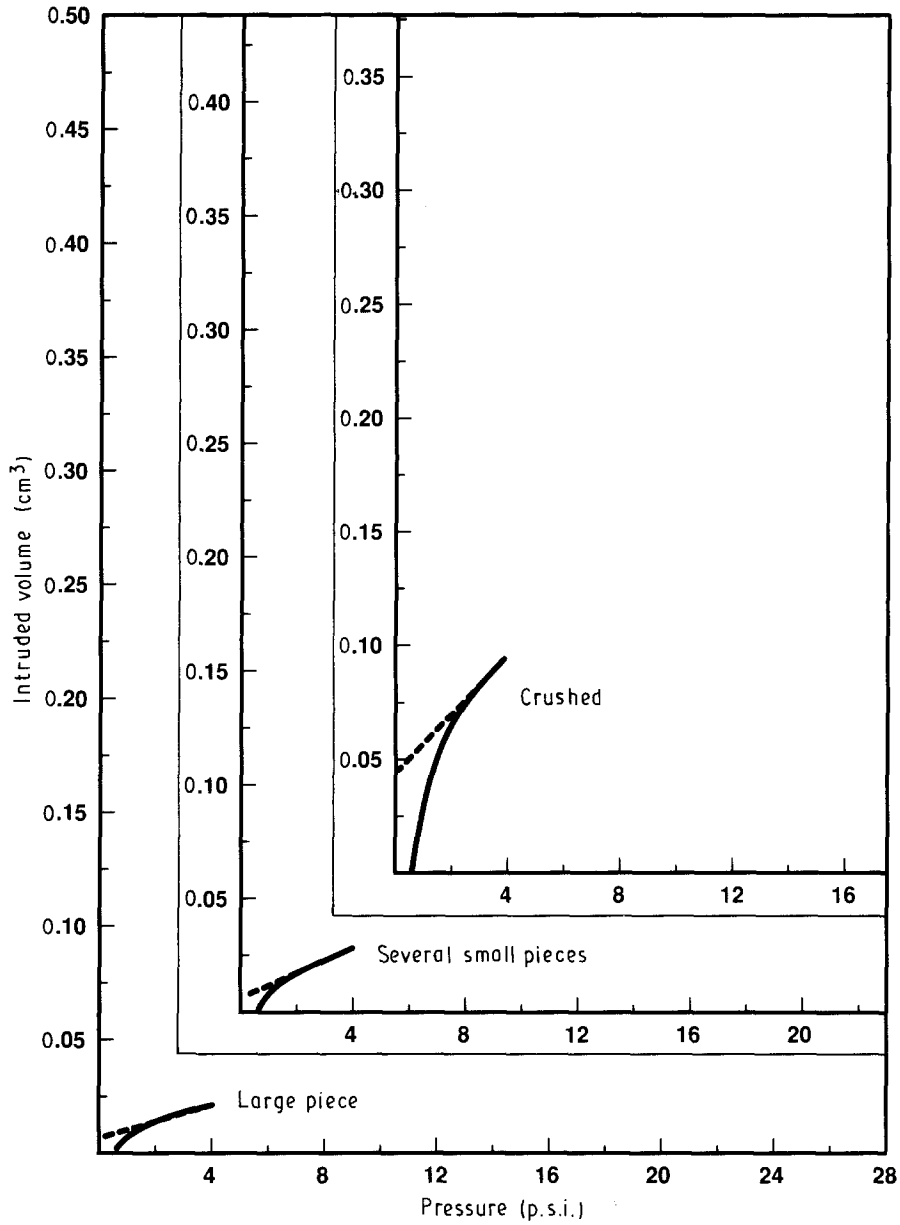

Figure 7 Surface filling artefact is demonstrated by obtaining an intrusion curve on samples prepared in different ways from the same carbon foam. The large piece shows little jump in the intrusion curve at the origin, the normal sized sample shows a small jump at the origin, and the sample consisting of many fine pieces shows a hugh jump at the origin.

calculation of the total void volume of the foam sample. The latter can be used to determine the sample density.

The second artefact often observed on the intrusion curves is due to bulk compression of the foam samples which occurs as the external surface of these relatively weak foams is pressurized. This is more of a problem with microcellular carbon foams than with other porous material such as glass or larger celled foams because high mercury pressures are required to enter the foam's small cells, and because of the low modulus of this type of material [12]. The bulk modulus is defined as

$$\kappa = -1/\Omega \, d\Omega/dP \qquad (13)$$

where Ω is the foam's total volume. For constant bulk modulus, the intrusion curve should have a linear region if plotted as intruded volume versus pressure. A typical linear region of this type is shown in the schematic drawing of Fig. 6 and in an actual intrusion curve in Fig. 4. As soon as mercury begins to enter the cells of the foam, however, no further compression would be expected to take place because the pressure would then be equal within and outside of the foam. From the slope of this linear region one can determine the bulk modulus of the foam. This effect must be eliminated from the calculated cell size distribution in order to differentiate between compression of the foam (a mechanical property) and intrusion into the cells of the foam (dependent upon cell size). It must be included in the total void volume calculation, however, which can be used to determine sample density.

It is well documented that many mercury intrusion curves show hysteresis upon depressurization [10]. One would expect little if any hysteresis if only bulk compression were occurring during pressurization. Fig. 8 shows three hysteresis curves obtained on the same carbon foam sample obtained at three intrusion pressures. In the linear region there is no significant hysteresis which is consistent with this being a region

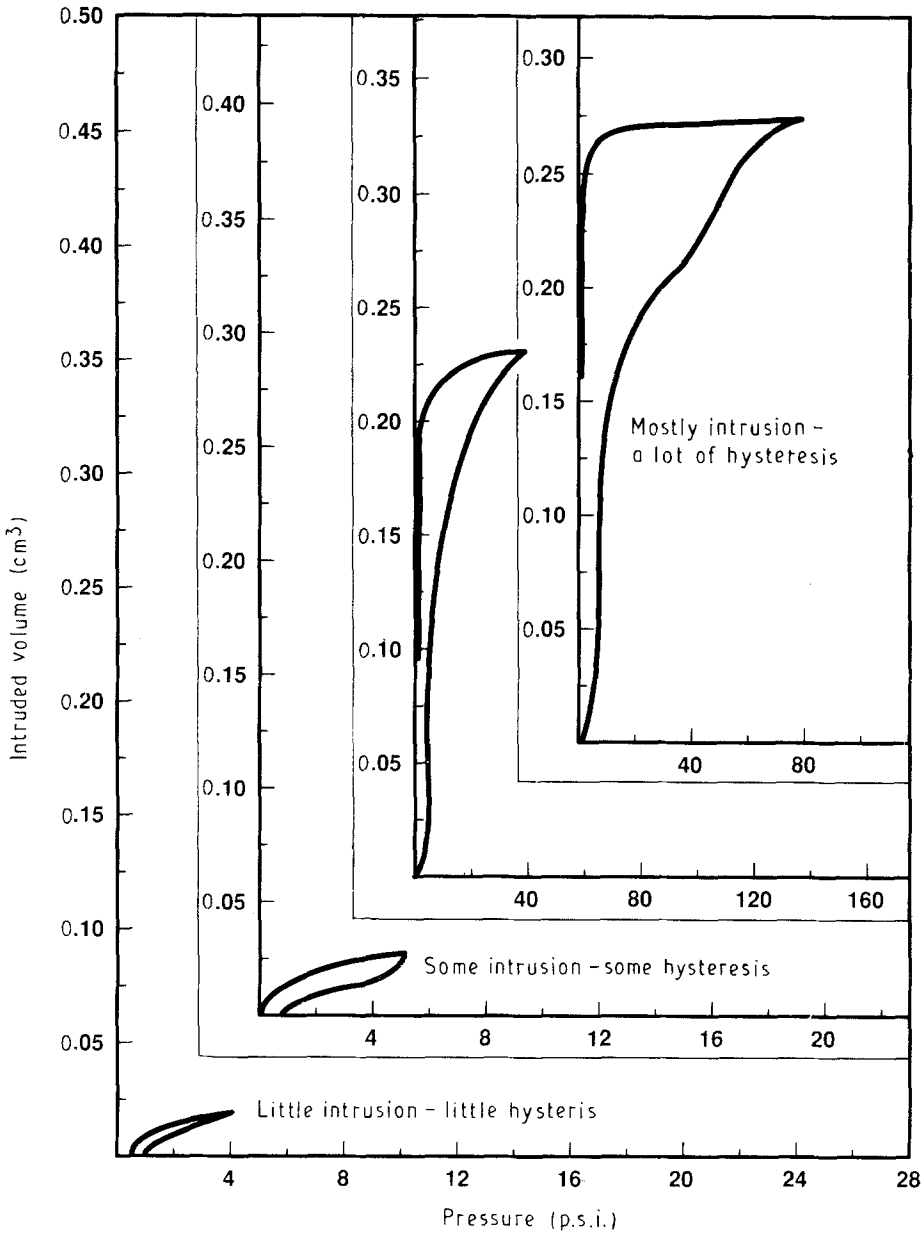

Figure 8 Hysteresis curves for a carbon foam pressurized to three different levels. No significant hysteresis occurs for the linear region of the intrusion curve corresponding to bulk compression. A large amount of hysteresis occurs after mercury begins to fill the cells of the foam.

of bulk compression. As soon as mercury begins to enter the cells of the foam (at the sharp upturn in the intrusion curve), then the hysteresis becomes significant.

The significance of removing these artefacts is great. If we analyse the intrusion curve of the foam described in Fig. 4 without removing the artefacts, we obtain 16.8 μm for the volume average cell size, $\langle d \rangle_V$, rather than 11.7 μm. This is an error of almost 44%. Most importantly, this error is different for each foam because it depends upon how the surface was prepared, how large the foam sample was, and the mechanical properties of the foam. On the other hand, if we ignore the artefacts, we get 6.65 μm for the surface area average cell size, $\langle d \rangle_S$, which is almost identical to the 6.62 μm obtained when the artefacts are removed. The surface area average cell size is very insensitive to the artefacts.

What remains after the artefacts have been removed from the intrusion curve are data corresponding to intrusion of mercury into the cells. These can potentially be used to quantify the cell-size-distributions. Prior to this, however, it is prudent to check on the validity of interpreting the intrusion data according to Equation 7. If bottleneck cells exist in the foam, then the intrusion pressure will correspond to the cell size of the neck and not the desired cell size. Fig. 9 shows two possible cell configurations which would yield very different results in a mercury porosimetry experiment. For the carbon microcellular foams analysed in this work, measurements of the surface areas from BET nitrogen adsorption and mercury porosimetry are in good agreement as is shown in Fig. 10. This implies an absence of bottleneck cells and justifies the interpretation of the cell size distributions based upon the mercury porosimetry data.

Figs 11 and 12 are mercury porosimetry intrusion curves and scanning electron photomicrographs of two microcellular carbon foams which have nearly the same density and cell-size-distribution. Also included on the intrusion curves are the statistical data described in Table I after proper accounting for the

artefacts. The mercury porosimetry results for these two similar foams are also nearly identical which indicates the validity of the technique. This is not so if the artefacts are included. In that case the volume average cell sizes are 5.52 and 6.66 μm for foams 704 and 491 rather than the corrected values of 2.88 and 2.87 μm, respectively. Not only would the reported values be in error by almost 100%, but more importantly, two nearly identical foams would have different values reported for this average cell size. As before, the

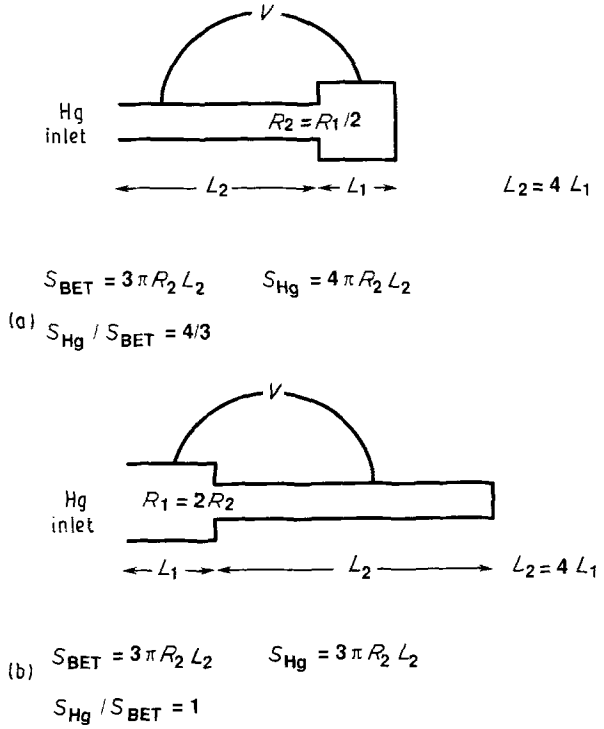

Figure 9 Possible cell morphologies and their result on interpreting mercury porosimetry intrusion curves. (a) For bottleneck cells a significant difference occurs in the surface area measure from BET nitrogen adsorption or mercury porosimetry. (b) For regular cells the surface area measurements will be the same.

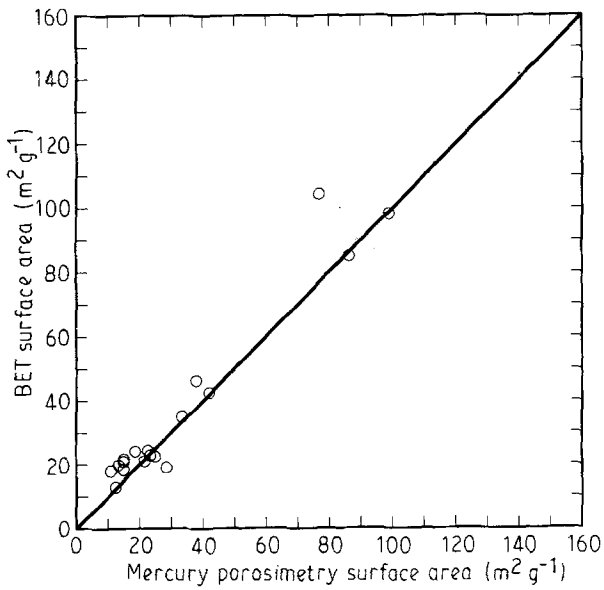

Figure 10 A comparison of the surface area per unit mass measured with BET nitrogen adsorption and mercury porosimetry on carbon microcellular foams. The close agreement justifies the interpretation of the mercury porosimetry data.

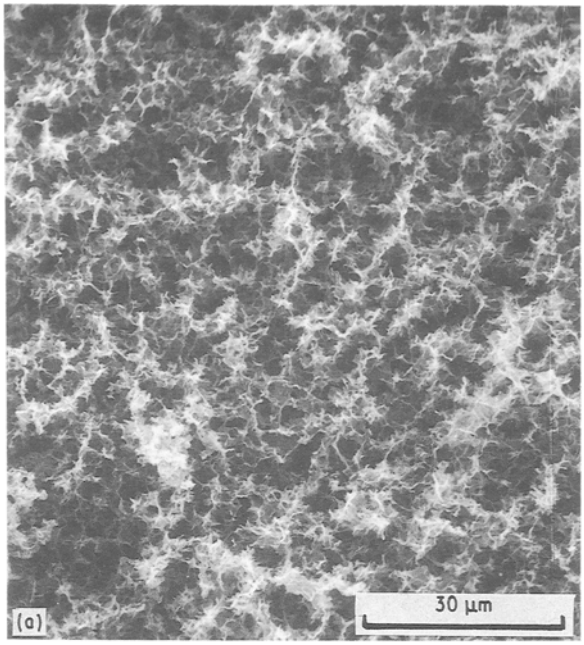

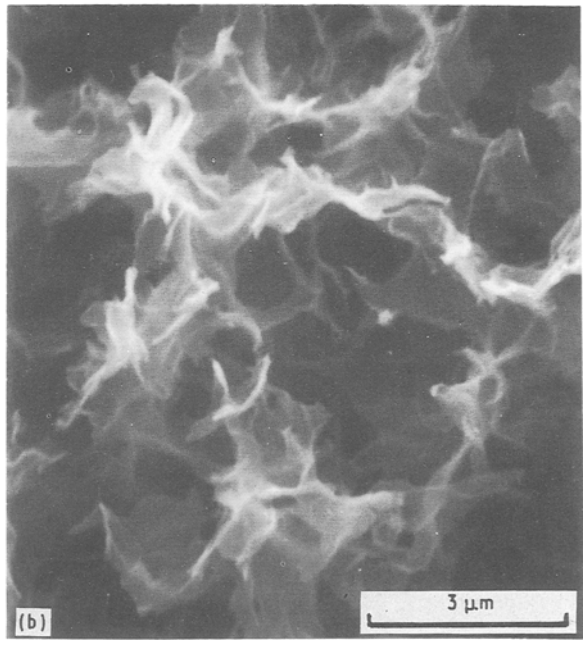

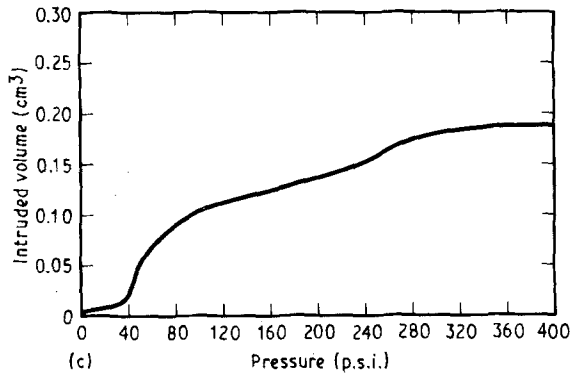

Figure 11 Mercury intrusion curve of a carbon microcellular foam of density 0.057 g cm^{-3}. The bimodal cell size distribution is evident both from the intrusion curve and from the photomicrographs. $\langle d \rangle_V = 2.88$ μm, $\langle d \rangle_S = 1.90$ μm, $\sigma_V / \langle d \rangle_V = 0.65$, $\rho_{Hg} = 57.3$ mg cm^{-3}.

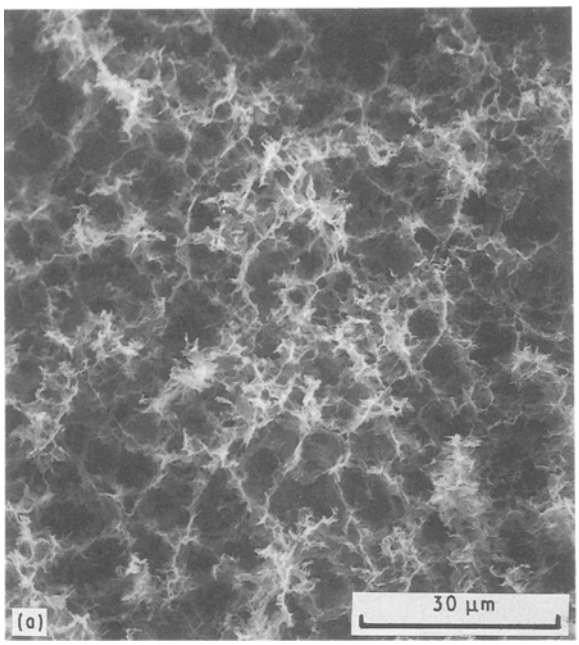

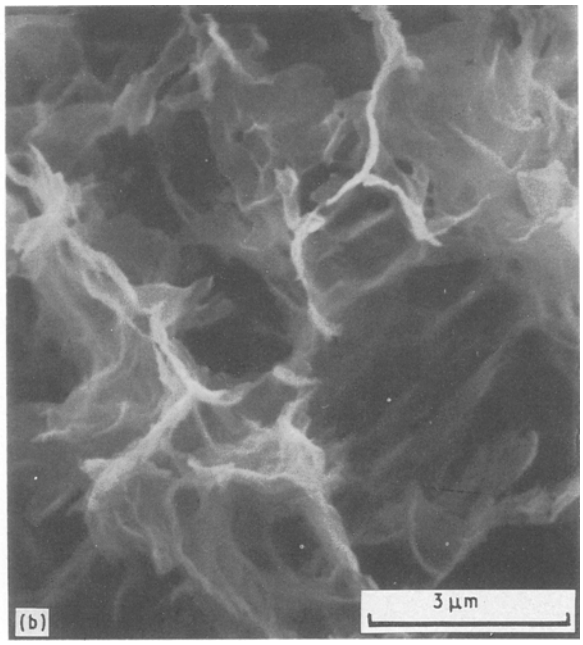

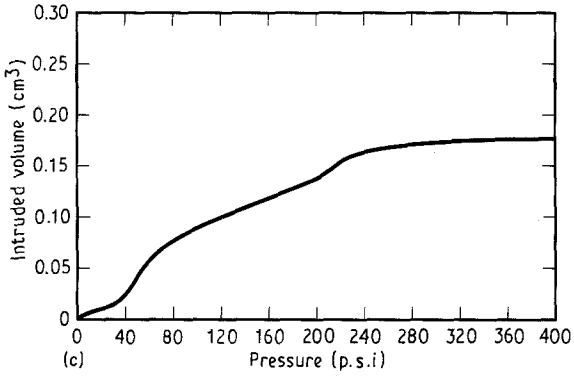

Figure 12 Mercury intrusion curve of a carbon foam which is nearly identical to that described in Fig. 11. Note that the analysis of the intrusion curve gives identical results to Fig. 11 which helps to validate the analysis. $\langle d \rangle_V = 2.87\ \mu m$, $\langle d \rangle_S = 2.07\ \mu m$, $\sigma_V/\langle d \rangle_V = 0.64$, $\rho_{Hg} = 57.4\ mg\,cm^{-3}$.

surface area average cell size is very insensitive to the artefacts. For foam 704 the corrected and uncorrected values of $\langle d \rangle_S$ are 1.90 and 1.96 μm. For foam 491 the corrected and uncorrected values of $\langle d \rangle_S$ are 2.07 and 2.13 μm. Fig. 13 shows the intrusion curve, scanning electron photomicrographs, and the statistical data for a larger cell sized foam. The density, which is identified as ρ_{Hg}, is based upon the total void volume of the foam (from the intrusion curve discounting the amount due to surface defects) and assuming that the volume of carbon is equal to the mass of carbon divided by the density (assumed to be $2.0\,g\,cm^{-3}$). The other reported density, ρ, is based upon weight and volume determinations on the foam. The good agreement between these two measurements supports the mercury intrusion results and implies that all of the pore volume was accessable to mercury. This foam's cell size distribution is also bimodal, as is seen both from the photomicrographs and the intrusion curve. The cell sizes determined from the intrusion curve are consistent with what is observed on the photomicrographs. Results for a finer celled carbon foam are shown in Fig. 14. This foam has a cell size distribution that is nearly monodisperse as indicated by the low standard deviation.

The value of being able objectively to quantify the cell size distribution of carbon microcellular foams can be demonstrated with an analysis of the bulk moduli. Bulk moduli as a function of foam density are shown in Fig. 15. The least squares fit line has a slope of 2.88, which implies that the bulk moduli are a strong function of foam density. This conclusion contradicts recent theories of the density dependence of the bulk moduli of foams. The theory of Warren and Kraynik [13] predicts that the bulk moduli are only linearly proportional to foam density, independent of foam cell size, but strongly dependent upon foam morphology (i.e. how the mass of the foam is distributed within the walls or struts of the foam). Therefore, one must ask whether our moduli measurements imply an actual density dependence or rather a dependence upon foam cell size or foam morphology, because they cannot be varied independently from the density. Fig. 16 shows the bulk moduli as a function of the volume average cell size. This plot reduces the data even better than does the plot of bulk moduli versus density. In fact quite a few of the foams tested had different densities but similar cell sizes. Results for these foams, Fig. 17, show that the bulk moduli are actually not very sensitive to the density (consistent with the Warren–Kraynik theory), but correlate well with the volume average cell size. In the carbon foams that we investigated the foam cell size is coupled to the foam morphology, i.e. as we change cell size we also change how the mass is distributed within the cells. Hence, our results may reflect a strong dependence of the bulk moduli on foam morphology, with the changing morphology being manifested in the changing values of the volume average cell sizes. All of the experimental results are summarized in Table II. Without a technique to characterize quantitatively and objectively the morphology of carbon microcellular foams, analyses such as these could not be

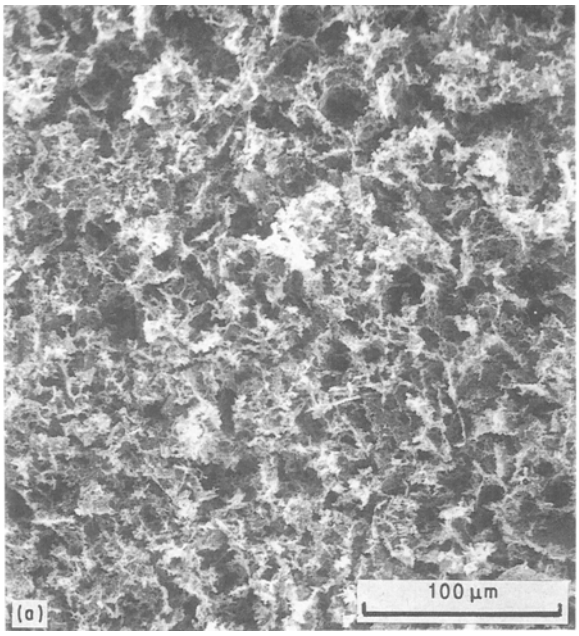

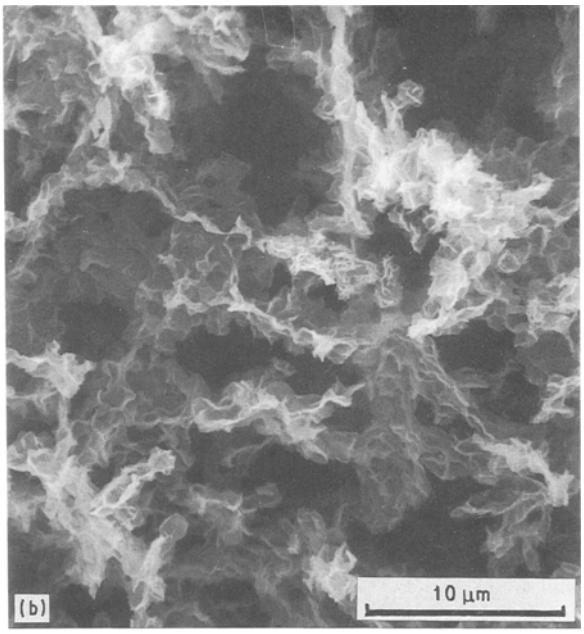

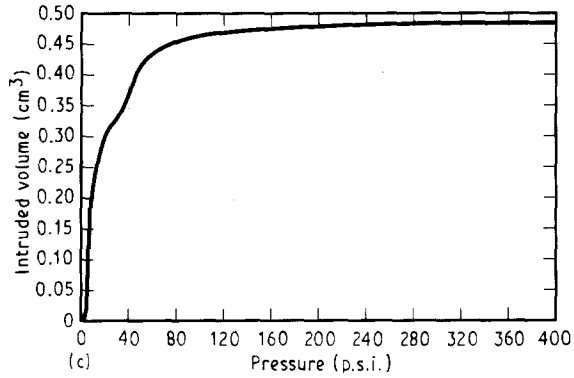

Figure 13 Mercury intrusion curve and scanning electron photomicrographs of a carbon foam with larger cell sizes. Note the good correlation of the sizes observed on the photomicrographs and those calculated from the intrusion curve. This foam also has a bimodal cell size distribution and a relatively large standard deviation, $\sigma_V/\langle d\rangle_V = 0.80$. Weight 0.0185 g, $\langle d\rangle_V = 20.46\ \mu m$, $\langle d\rangle_S = 8.24\ \mu m$, $\rho_{Hg} = 37.9\ mg\,cm^{-3}$, $\rho_{Hg}/\rho = 1.04$.

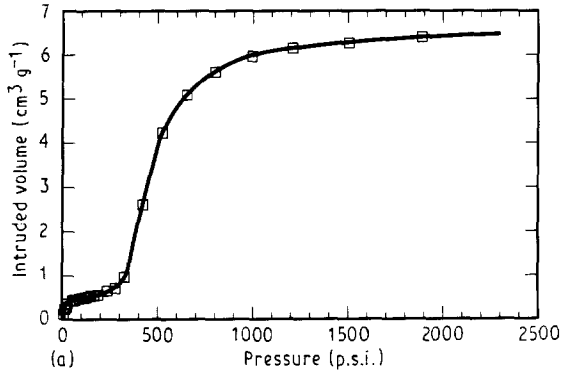

Figure 14 (a) Mercury intrusion curve and (b) scanning electron photomicrograph of a carbon foam with a small cell size. This foam is nearly monodisperse and has a low standard deviation, $\sigma_V/\langle d\rangle_V = 0.36$, $\langle d\rangle_V = 0.53\ \mu m$, $\langle d\rangle_S = 0.36\ \mu m$, $\rho_{Hg} = 0.147\ g\,cm^{-3}$.

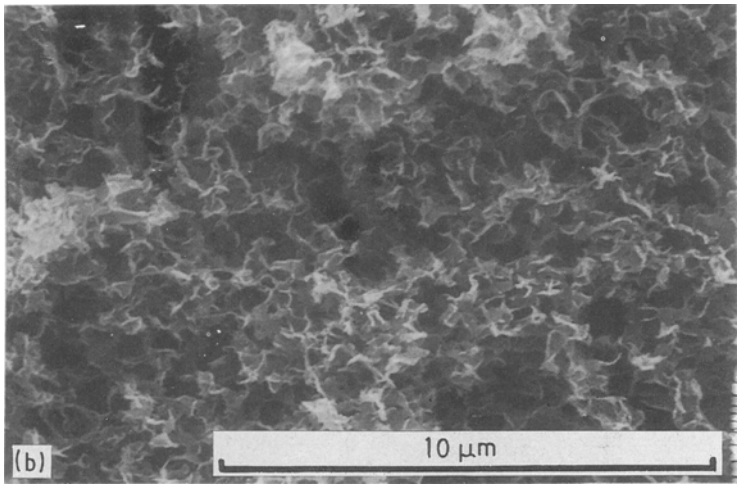

accomplished, and one might incorrectly conclude that bulk moduli are a strong function of foam density.

5. Conclusions

BET surface area measurements and mercury porosimetry are both useful techniques to characterize quantitatively open-celled carbon foam morphologies. Neither technique requires any a priori morphological assumption. The ratio of a volume average cell size (obtainable from mercury porosimetry) to a surface area average cell size (obtainable from both BET nitrogen adsorption and mercury porosimetry) is a good measure of the width of the cell size distribution. Artefacts must be eliminated from the mercury intrusion curve prior to the cell size distribution analysis. Without this removal, the artefacts can dominate the calculated results. The surface area average cell size is, however, insensitive to these artefacts. If uncertainty exists about the artefacts, then the surface area average is a more reasonable cell size to report. The surface area average cell size is also the easiest to obtain. The bulk modulus of carbon microcellular foams can be determined from mercury intrusion experiments. It is shown that the bulk modulus is a strong function of foam morphology as manifested by the volume average cell size but only weakly dependent upon foam

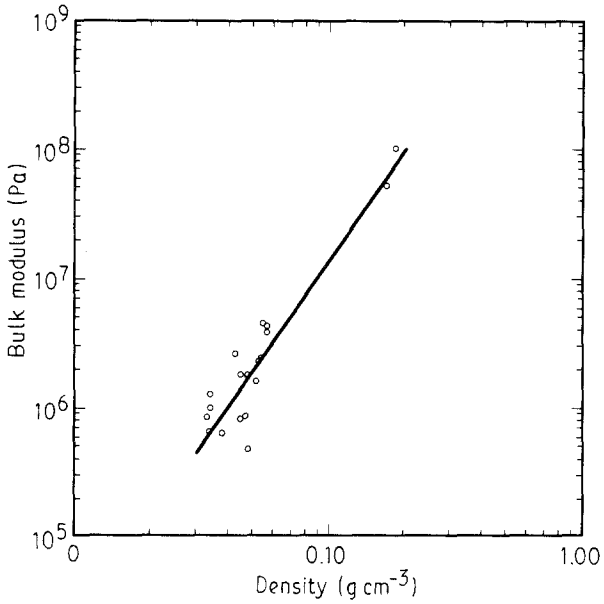

Figure 15 Bulk modulus as a function of carbon foam density. The least squares fit line (——) has a slope of 2.88.

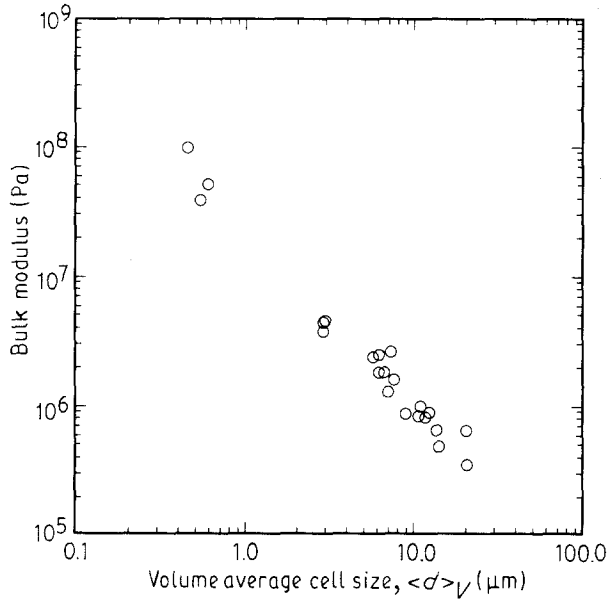

Figure 16 Bulk modulus as a function of the volume average cell size for all foam densities.

TABLE II Summary of mercury porosimetry and BET nitrogen adsorption analysis for all carbon foams tested

Foam	Density (g cm^{-3})	S_{BET} (m^2 g^{-1})	S_{Hg} (m^2 g^{-1})	S_{Hg}/S_{BET}	κ (10^{-5} Pa)	$\langle d \rangle_S$ (μm)	$\langle d \rangle_V$ (μm)	$\sigma_V/\langle d \rangle_V$	$\langle d \rangle_V/\langle d \rangle_S$
1431	0.033	19.0	28.4	1.50	8.39	4.26	10.6	0.74	2.50
1299	0.034	34.7	33.4	0.96	9.90	3.51	10.9	0.93	3.11
1430	0.034	22.1	24.7	1.12	6.49	4.72	13.6	0.75	2.89
1341	0.034	42.5	41.8	0.98	12.8	2.79	6.95	0.69	2.49
1156	0.038	18.2	12.8	0.70	6.43	8.24	20.5	0.80	2.48
1155	0.039	19.2	13.2	0.69	3.43	7.76	20.7	0.83	2.67
1361	0.043	21.0	21.3	1.01	26.3	4.38	7.14	0.64	1.63
1279	0.044	12.7	12.1	0.95	8.66	7.60	12.2	0.74	1.60
1401	0.045	22.8	23.8	1.04	18.3	3.73	6.17	0.67	1.65
1260	0.045	21.5	13.3	0.62	8.22	6.62	11.7	0.69	1.77
1406	0.047	18.1	14.9	0.82	8.57	5.75	8.89	0.70	1.55
1359	0.048	23.9	22.9	0.96	18.1	3.68	6.40	0.68	1.74
1261	0.048	17.7	10.9	0.61	4.73	7.62	14.1	0.69	1.85
1353	0.052	20.0	14.6	0.73	16.1	5.24	7.64	0.59	1.46
1370	0.053	23.8	18.7	0.78	23.4	4.03	5.68	0.58	1.41
906	0.054	20.4	14.9	0.73	24.5	4.97	6.12	0.50	1.23
1389	0.055	46.4	37.6	0.81	45.5	1.95	2.91	0.64	1.49
704	0.057	53.9	36.8	0.68	43.6	1.90	2.88	0.65	1.52
491	0.057	34.1	33.7	0.99	38.6	2.07	2.87	0.64	1.39
P411	0.147	105	76.2	0.73	402	0.36	0.53	0.36	1.50
P410	0.168	84.8	85.9	1.01	527	0.28	0.59	0.42	2.15
P420	0.182	98.0	98.1	1.00	1014	0.22	0.45	0.34	1.99

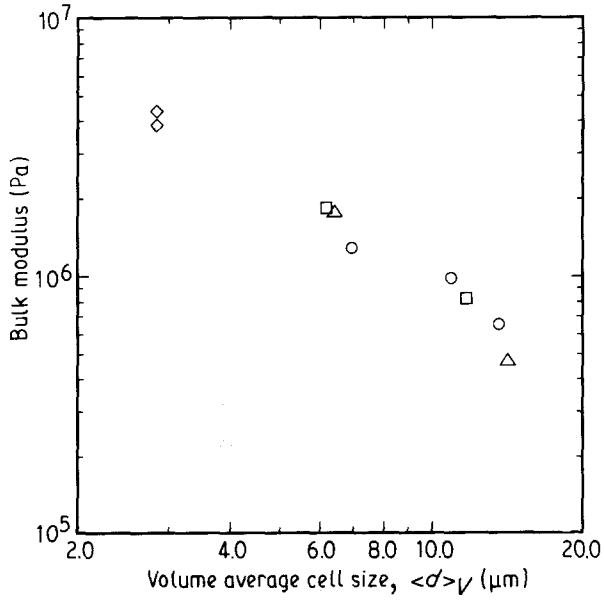

Figure 17 Bulk modulus as a function of the volume average cell size for different groupings of carbon foam densities (g cm^{-3}): (◇) 0.057, (△) 0.048, (□) 0.045, (○) 0.034.

density. Such an analysis would be impossible without techniques to characterize quantitatively and objectively the morphology of carbon microcellular foams.

Acknowledgements

We thank L. Salgado and E. Russick for preparing the foams used in this study, E. Russick for performing the BET nitrogen adsorption and mercury porosimetry experiments, R. Pekala for obtaining the high-pressure mercury porosimetry for our use and D. Huskisson and B. McKenzie for performing the scanning electron microscopy. This work performed at Sandia National Laboratories for the US Department of Energy under Contract no. DE-A304-76DP00789.

References

1. C. ARNOLD JR, J. H. AUBERT, R. L. CLOUGH, P. B. RAND and A. P. SYLWESTER, US Pat. no. 4 832 881 (1989).
2. A. P. SYLWESTER, J. H. AUBERT, P. B. RAND, C. ARNOLD JR and R. L. CLOUGH, *ACS Polym. Mater. Sci. Engng* **57** (1987) 113.
3. R. W. HOPPER and R. W. PEKALA, US Pat. no. 4 756 898 (1988).
4. R. W. PEKALA and R. H. HOPPER, *J. Mater. Sci.* **22** (1987) 1840.
5. R. W. PEKALA and R. E. STONE, *ACS Polym. Prepr.* **29** (1988) 204.
6. J. H. AUBERT and R. L. CLOUGH, *Polymer* **26** (1985) 2047.
7. J. B. DONNET and R. C. BANSAL (Eds), "Carbon Fibers" (Marcel Dekker, New York, NY, 1984).
8. J. H. AUBERT, *J. Cellular Plastics* **24** (1988) 132.
9. E. E. UNDERWOOD, "Quantitative Stereology" (Addison-Wesley, Reading, MA, 1970).
10. S. LOWELL and J. E. SHIELDS, "Powder Surface Area and Porosity", 2nd Edn (Chapman and Hall, NY, 1984).
11. R. B. BIRD, W. E. STEWART and E. N. LIGHTFOOT, "Transport Phenomena" (Wiley, New York, NY, 1960).
12. C. L. JACKSON, M. T. SHAW and J. H. AUBERT, *Polymer* **32** (1990) 221.
13. W. E. WARREN and A. M. KRAYNIK, *J. Appl. Mech.* **110** (1988) 341.

Received 23 April
and accepted 6 November 1990